Cruise report, expedition 64PE-549
Texel – Texel, the Netherlands (22-09 – 08-10-2025)

Helge Niemann[1,2], Rosanne Huybens[3], Annalisa Delre[1], Laurens van der Marel[1,2], Martin Whilpshaar[3], Barend van Engelenburg[4]

[1]Royal Netherlands Institute for Sea Research (NIOZ)
[2]Utrecht University
[3]TNO Geological Survey of the Netherlands
[4]SoDM

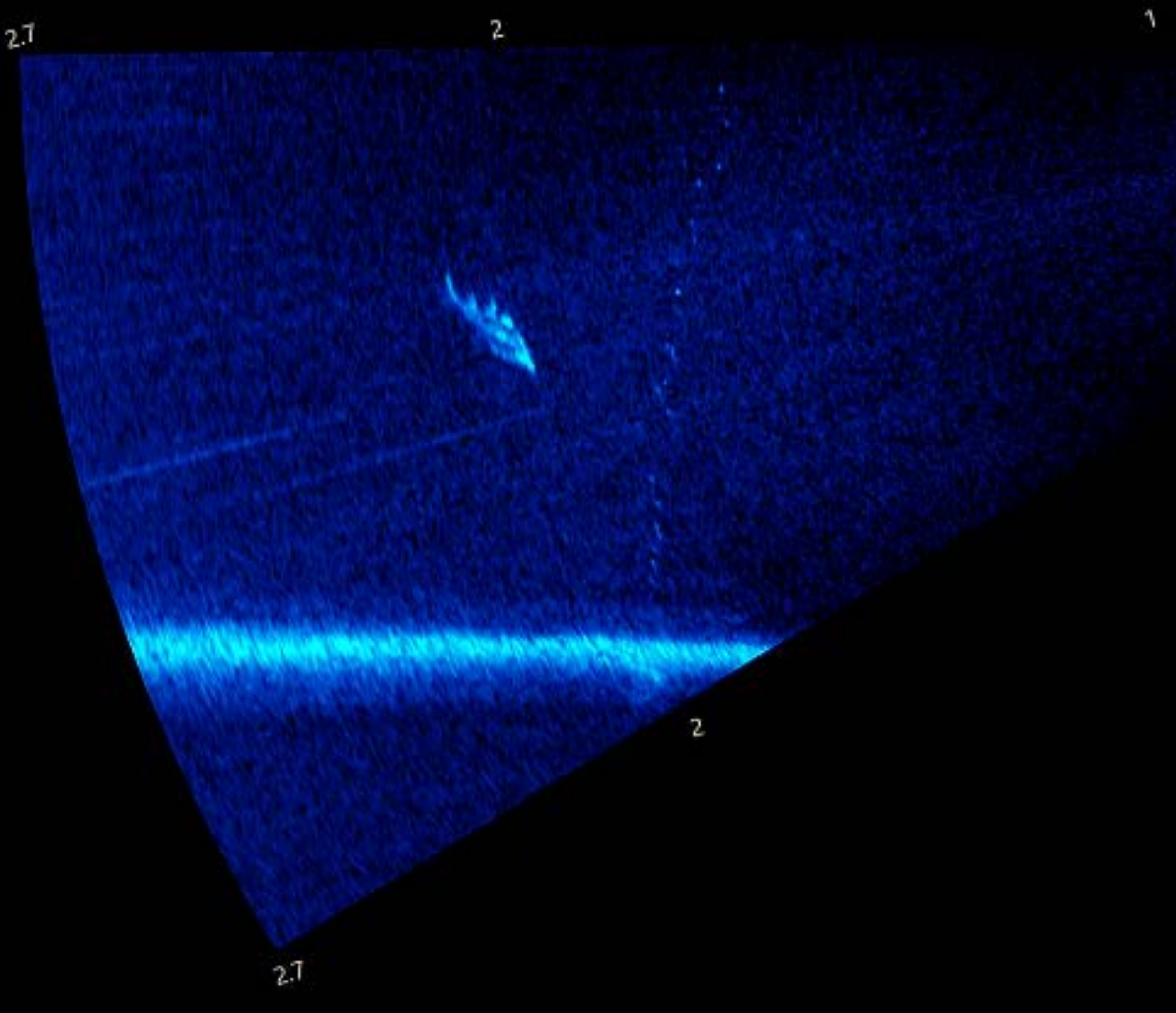

Contents

1. General introduction and expedition goals

Helge Niemann, Chief Scientist

Methane (CH_4) is an important greenhouse gas, that is 32 times more potent than CO_2 on a time horizon of 100 years (Etminan et al., 2016). Though the half-life of atmospheric methane is relatively short (~ 9 years), CH_4 concentrations in the atmosphere have risen drastically to current values of ~ 1.9 ppm; i.e. ~ 2.5-fold higher compared to preindustrial values (IPCC, 2021). The exact mechanisms behind this increase are not fully understood, yet it is clear that the increase in the atmospheric methane budget is caused by anthropogenic sources (Nisbet et al., 2019; IPCC, 2021; Saunois et al., 2025); together, these amount to 345 - 409 Tg yr^{-1}. Natural CH_4 sources are overall on a similar scale contributing about 40% (195 - 457 Tg yr^{-1}) to the total atmospheric budget (540 – 865 Tg yr^{-1}).

Though it is likely that the overall contribution of the Ocean to the atmospheric methane budget is comparably small, ocean budget estimates vary considerably. Shelf seas for example are with 6 - 22 Tg yr^{-1} the main contributor of natural oceanic methane emission to the atmosphere though the shelf only accounts for 8 - 10 % of the global ocean surface (Weber et al., 2019; Saunois et al., 2020). Compared to the open ocean, shelf seas are characterized by high nutrient loads, high primary production, high sedimentation rates and subsequent burial of dead organic matter to the seabed. This leads to elevated methane production in sediments by microbial or thermogenic processes (Reeburgh, 2007). Methane emission related to offshore industries on the other hand are not well constrained but expected to be substantial (Pühl et al., 2024; IEA, 2025) . However, methane in shelf sea sediments is of commercial value and thus extracted. After exploitation, wells are sealed to prevent leakage, but recent investigations in the UK and German sector of the North Sea by Vielstädte et al. (2017), Böttner et al. (2020) and de Bruin (Bruin et al., 2025) however, found acoustic flares in the water column in vicinity of well heads; these acoustic features are caused by plumes of rising bubbles emanating from the sea floor. Such flares were almost always found when the well heads were in close vicinity to so-called bright spots in seismic data. Bright spots are caused by high amplitude response in sound velocity of the subsurface, e.g. triggered by the presence of shallow gas. The studies by Vielstädte et al. (2017), Böttner et al. (2020) could not fully clarify why the location of sea floor gas release was often at some distance from the well head (i.e. the leak-tightness of the well head seal itself was not necessarily compromised). However, the statistical co-occurrence of flares and (abandoned) wells suggested a causality. The available investigations also suggest that the frequency of plumes in UK and Norwegian sector might be higher than in the Dutch sector of the North Sea (Bruin et al., 2025).

The Dutch sector of the North Sea is rich in shallow and deep subsurface methane. The deep methane is extracted from multiple active wells and many more wells are abandoned and sealed. With respect to the previous findings (Vielstädte et al., 2017; Böttner et al., 2020; Bruin et al., 2025) this raises the questions:

- **if and how frequent gas release occurs at or in the vicinity of (abandoned) wells in the Dutch sector of the North Sea;**
- **if the gas release is caused by the previous drilling and/or inappropriate sealing attempts.**

Furthermore, leaking offshore wells, may form an anthropogenic analogue to natural cold seeps. At cold seeps, methane migrates upwards through cracks and fissures in the sea bed and may be released as dissolved or free gas into the water column (James et al., 2016). Cold seeps are thus methane hotspot point sources, and they occur frequently along shelf seas across the globe (Steinle et al., 2015), promoting methane transport to the atmosphere (McGinnis et al., 2006; Deimling et al., 2011).

Nevertheless, a substantial amount of the water column methane content at cold seeps is consumed by aerobic methane oxidizing bacteria (MOB) that mediate the aerobic oxidation of methane (MOx; Reeburgh 2007).

This raises a further question:

- **if and how much of the released CH_4 is microbially consumed in the water column and how much is ultimately released to the atmosphere.**

With these questions in mind, NIOZ & TNO have been commissioned by SoDM to investigate CH_4 dynamics at abandoned wells in the Dutch North Sea. In the first phase of this project, a first research expedition with R/V Pelagia was carried out in summer 2022 (June 2nd to 22nd (cruise PE-503). During this cruise, around 50 well locations were investigated for leakage and ranked for further in-depth investigation (Bruin et al., 2025) . These investigations were aimed to take place during well mixed and fully stratified water column conditions, as this can severely influence methane release to the atmosphere (Steinle et al., 2016; Groot et al., 2024). An expedition in 2024 (PE-525) was thus conducted during fully mixed and quite stormy conditions.

The current cruise, PE-549, was carried out to further investigate the intermittency of seafloor methane release at the B17-05 and B17-04 sites visited during previous expeditions. In addition, we aimed to survey other suspended and abandoned well locations and assess potential methane emissions using echosounder-based techniques and direct observations with a remotely operated vehicle (ROV). We also tested new approaches for calibrating sonar-based methods to quantify methane release from the seafloor. Finally, we measured methane concentrations in the water column in situ using laser absorption spectrometry and/or collected discrete water samples for concentration and stable carbon isotope analysis.

Bibliography

Böttner, C., Haeckel, M., Schmidt, M., Berndt, C., Vielstädte, L., Kutsch, J.A., Karstens, J., Weiß, T., 2020. Greenhouse gas emissions from marine decommissioned hydrocarbon wells: leakage detection, monitoring and mitigation strategies. International Journal of Greenhouse Gas Control 100, 103119.

de Bruin, G. de, Stigter, H. de, Diaz, M., Delre, A., Velzeboer, I., Versteijlen, N., Niemann, H., Wilpshaar, M., Reichart, G.J., 2025. Methane leakage from abandoned wells in the Dutch North Sea. Marine and Petroleum Geology 171, 107184.

Deimling, J.S. von, Rehder, G., Greinert, J., McGinnnis, D.F., Boetius, A., Linke, P., 2011. Quantification of seep-related methane gas emissions at Tommeliten, North Sea. Continental Shelf Research 31, 867–878.

Etminan, M., Myhre, G., Highwood, E.J., Shine, K.P., 2016. Radiative forcing of carbon dioxide, methane, and nitrous oxide: A significant revision of the methane radiative forcing. Geophysical Research Letters 43, 12,614-12,623.

de Groot, T.R., Menoud, M., Bleijswijk, J. van, Leeuwen, S.M. van, Molen, J. van der, Hernando-Morales, V., Czerski, H., Maazallahi, H., Walter, S., Rush, D., Röckmann, T., Niemann, H., 2024. Tidal and seasonal influence on cold seep activity and methanotroph efficiency in the North Sea. Communications Earth & Environment 5, 368.

IEA, 2025. Global Methane Tracker 2025. IEA Publications.

IPCC, 2021. Climate Change 2021: The Physical Science Basis. Contribution of Working Group I to the Sixth Assessment Report of the Intergovernmental Panel on Climate Change, Chemistry International. Cambridge University Press, Cambridge, United Kingdom and New York, NY, USA. doi:10.1515/ci-2021-0407

James, R.H., Bousquet, P., Bussmann, I., Haeckel, M., Kipfer, R., Leifer, I., Niemann, H., Ostrovsky, I., Piskozub, J., Rehder, G., Treude, T., Vielstädte, L., Greinert, J., 2016. Effects of climate change on methane emissions from seafloor sediments in the Arctic Ocean: A review. Limnology and Oceanography 61, S283–S299.

McGinnis, D.F., Greinert, J., Artemov, Y., Beaubien, S.E., Wuest, A., 2006. Fate of rising methane bubbles in stratified waters: How much methane reaches the atmosphere? J. Geophys. Res.-Oceans 111, 15.

Nisbet, E.G., Manning, M.R., Dlugokencky, E.J., Fisher, R.E., Lowry, D., Michel, S.E., Myhre, C.L., Platt, S.M., Allen, G., Bousquet, P., Brownlow, R., Cain, M., France, J.L., Hermansen, O., Hossaini, R., Jones, A.E., Levin, I., Manning, A.C., Myhre, G., Pyle, J.A., Vaughn, B.H., Warwick, N.J., White, J.W.C., 2019. Very Strong Atmospheric Methane Growth in the 4 Years 2014–2017: Implications for the Paris Agreement. Global Biogeochemical Cycles 33, 318–342.

Pühl, M., Roiger, A., Fiehn, A., Negron, A.M.G., Kort, E.A., Schwietzke, S., Pisso, I., Foulds, A., Lee, J., France, J.L., Jones, A.E., Lowry, D., Fisher, R.E., Huang, L., Shaw, J., Bateson, P., Andrews, S., Young, S., Dominutti, P., Lachlan-Cope, T., Weiss, A., Allen, G., 2024. Aircraft-based mass balance estimate of methane emissions from offshore gas facilities in the southern North Sea. Atmospheric Chemistry and Physics 24, 1005–1024.

Reeburgh, W.S., 2007. Oceanic methane biogeochemistry. Chemical Reviews 107, 486–513.

Saunois, M., Martinez, A., Poulter, B., Zhang, Z., Raymond, P.A., Regnier, P., Canadell, J.G., Jackson, R.B., Patra, P.K., Bousquet, P., Ciais, P., Dlugokencky, E.J., Lan, X., Allen, G.H., Bastviken, D., Beerling, D.J., Belikov, D.A., Blake, D.R., Castaldi, S., Crippa, M., Deemer, B.R., Dennison, F., Etiope, G., Gedney, N., Höglund-Isaksson, L., Holgerson, M.A., Hopcroft, P.O., Hugelius, G., Ito, A., Jain, A.K., Janardanan, R., Johnson, M.S., Kleinen, T., Krummel, P.B., Lauerwald, R., Li, T., Liu, X., McDonald, K.C., Melton, J.R., Mühle, J., Müller, J., Murguia-Flores, F., Niwa, Y., Noce, S., Pan, S., Parker, R.J., Peng, C., Ramonet, M., Riley, W.J., Rocher-Ros, G., Rosentreter, J.A., Sasakawa, M., Segers, A., Smith, S.J., Stanley, E.H., Thanwerdas, J., Tian, H., Tsuruta, A., Tubiello, F.N., Weber, T.S., Werf, G.R. van der, Worthy, D.E.J., Xi, Y., Yoshida, Y., Zhang, W., Zheng, B., Zhu, Qing, Zhu, Qiuan, Zhuang, Q., 2025. Global Methane Budget 2000–2020. Earth System Science Data 17, 1873–1958.

Saunois, M., Stavert, A.R., Poulter, B., Bousquet, P., Canadell, J.G., Jackson, R.B., Raymond, P.A., Dlugokencky, E.J., Houweling, S., Patra, P.K., Ciais, P., Arora, V.K., Bastviken, D., Bergamaschi, P., Blake, D.R., Brailsford, G., Bruhwiler, L., Carlson, K.M., Carrol, M., Castaldi, S., Chandra, N., Crevoisier, C., Crill, P.M., Covey, K., Curry, C.L., Etiope, G., Frankenberg, C., Gedney, N., Hegglin, M.I., Höglund-Isaksson, L., Hugelius, G., Ishizawa, M., Ito, A., Janssens-Maenhout, G., Jensen, K.M., Joos, F., Kleinen, T., Krummel, P.B., Langenfelds, R.L., Laruelle, G.G., Liu, L., Machida, T., Maksyutov, S., McDonald, K.C., McNorton, J., Miller, P.A., Melton, J.R., Morino, I., Müller, J., Murguia-Flores, F., Naik, V., Niwa, Y., Noce, S., O'Doherty, S., Parker, R.J., Peng, C., Peng, S., Peters, G.P., Prigent, C., Prinn, R., Ramonet, M., Regnier, P., Riley, W.J., Rosentreter, J.A., Segers, A., Simpson, I.J., Shi, H., Smith, S.J., Steele, L.P., Thornton, B.F., Tian, H., Tohjima, Y., Tubiello, F.N., Tsuruta, A., Viovy, N., Voulgarakis, A., Weber, T.S., Weele, M. van, Werf, G.R. van der, Weiss, R.F., Worthy, D., Wunch, D., Yin, Y., Yoshida, Y., Zhang, W., Zhang, Z., Zhao, Y., Zheng, B., Zhu, Qing, Zhu, Qiuan, Zhuang, Q., 2020. The Global Methane Budget 2000–2017. Earth System Science Data 12, 1561–1623.

Steinle, L., Graves, C.A., Treude, T., Ferre, B., Biastoch, A., Bussmann, I., Berndt, C., Krastel, S., James, R.H., Behrens, E., Boning, C.W., Greinert, J., Sapart, C.-J., Scheinert, M., Sommer, S., Lehmann, M.F., Niemann, H., 2015. Water column methanotrophy controlled by a rapid oceanographic switch. Nature Geoscience 8, 378–382.

Steinle, L., Schmidt, M., Bryant, L., Haeckel, M., Linke, P., Sommer, S., Zopfi, J., Lehmann, M.F., Treude, T., Niemannn, H., 2016. Linked sediment and water-column methanotrophy at a man-made gas blowout in the North Sea: Implications for methane budgeting in seasonally stratified shallow seas. Limnology and Oceanography 61, 367–386.

Vielstädte, L., Haeckel, M., Karstens, J., Linke, P., Schmidt, M., Steinle, L., Wallmann, K., 2017. Shallow Gas Migration along Hydrocarbon Wells–An Unconsidered, Anthropogenic Source of Biogenic Methane in the North Sea. Environmental Science & Technology 51, 10262–10268.

Weber, T., Wiseman, N.A., Kock, A., 2019. Global ocean methane emissions dominated by shallow coastal waters. Nature Communications 10, 4584.

2. Geographical area

Helge Niemann, Chief Scientist

Al sampling during PE-549 was conducted in the North Sea, within the EEZ of the Netherlands (Figure 1). This region features several thermogenic gas fields but also pockets of shallow gas and gas is exploited from numerous wells (www.nlog.nl). Water depth in this area is mostly 20 - 45 m. In total we conducted 95 single stations. Sonar observations were conducted at 110 well surface locations, while ROV observations were focused on locations B17-05, B17-04, K06-01 and L08-P-01/02/03/05. A bubble generator was deployed at location B17-05 and close to K10-C-01 and E11-01. Of the 110 well locations, B17-01, B17-03, B17-04 and B17-05 were visited already in during previous cruises. A complete station list and a full list of the visited wells is presented in the appendix.

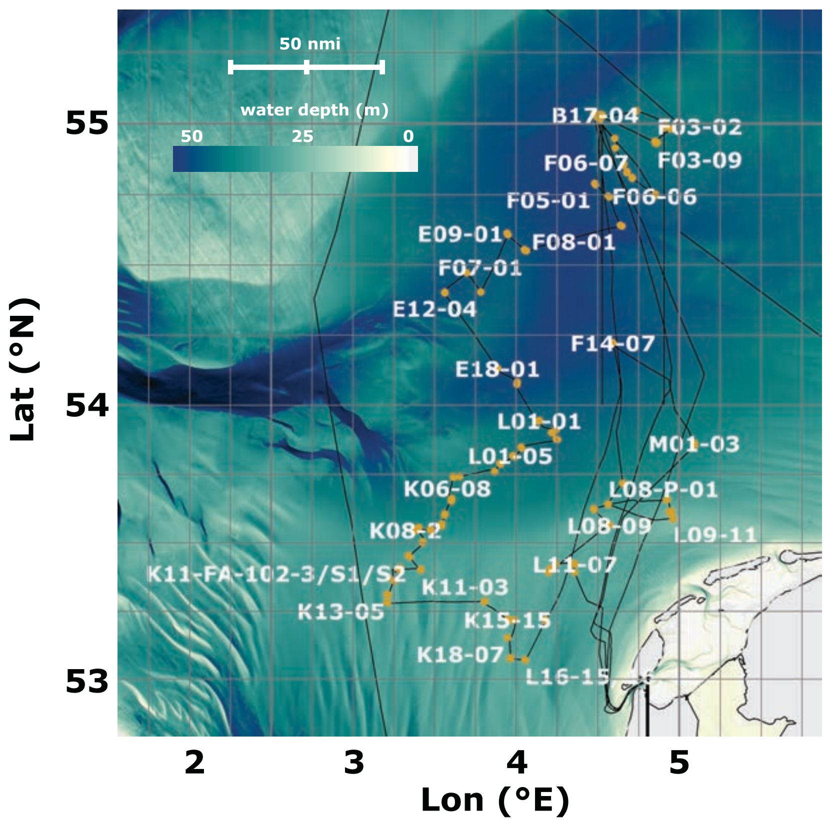

Figure 1 Area of investigation during PE-549. Single stations are highlighted as an orange dot, while the cruise track is indicated as a black line.

3. Bubbles in the water column

Rosanne Huybens, Laurens van der Marel, Martin Wilpshaar

3.1 Echosounder-based detection of bubbles

Both a single and a multi beam echo sounder were used to study the water column for methane bubbles rising from the seafloor and for seafloor features. On 114 locations the multibeam was used with a wide swath (detection mode) to detect bubbles. This was done by sailing parallel lines with a length of roughly 200 meters and distance between the lines that was roughly equal to the water depth. The goal was to measure an area of 200 by 250 meters with 50% overlap of the lines on both sides, as the side lobe image was not of high enough quality for bubble detection. With a water depth of 50 meters five lines were sailed in a 'paperclip', if the sea was significantly shallower one or two lines would be sailed extra. The sailing speed was aimed to be 2 knots to allow sufficient data points to be recorded within the water column needed for proper statistical analyses of the reflection strength.

When bubbles were suspected at a new location, more lines were sailed with the narrow swath multibeam (quantification mode) and the single beam was used, too. At locations where bubbles were found during previous methane expeditions, two other configurations of lines were sailed. Firstly, two boxes (~0.75 × 0.75 nmi) filled with lines were sailed over shallow gas leakage areas around (i) B17-03 and B17-05 as well as (ii) over B17-04. This was done to check how many plumes were active and at what locations compared to previous observations. Secondly, at B17-03, we sailed repeated lines over the location to investigate seepage intermittency.

3.1.1 Ships mounted single beam Echo sounder

The EK80 is a system consisting of one or multiple transducers with centre frequencies ranging from 18 to 333 kHz. For this study a mobile system, installed on the port side measurement pole of the vessel, was used consisting of a wide band transceiver (WBT mini) and two transducers with nominal frequencies of 70 and 200 kHz (Simrad ES70-7C and ES200-7C respectively). The ES70-7C is a split beam transducer with a bandwidth of 45-90 kHz and a circular beamwidth of 7 degrees. The ES200-7C also is a 7 degrees split beam transducer. The bandwidth for this device ranges from 160 to 260 kHz. Position and motion data is stored within the datafile. This information is supplied by the Seapath380/MRU 5+ ships attitude system. The position of the transducers on the pole relative to the GNSS antenna and MRU5+ is included in the final positioning of the data. Data were recorded using the matching Kongsberg EK80 software. The data was stored in raw format.

3.1.2 Ships mounted multi beam Echo sounder

All surveys were carried out with a high-resolution Kongsberg EM2040MKII mobile multibeam echosounder mounted on the ships port side measuring pole. The EM2040MKII is a high resolution 200-700 kHz shallow water multibeam. Experience during the 2022 cruise for this project has shown that running it at a frequency of 300 kHz gives the best possible results. Therefore, also this year surveys were carried out using 300 kHz. The beam opening angle at this frequency is 1° for the transmitter and receiver beam angle respectively. The swath opening angle during detection mode was fixed at 55° port side and starboard side. During quantitative mode the swath opening angle was set to 45° port side and starboard side. An offset calibration was carried out at the beginning of the cruise. However, since the pole did not return to exactly the same position at each deployment, this resulted in variable angular offsets for subsequent runs (i.e. a horizontal seabed appears to be dipping a couple of degrees). Therefore, a correction must be applied to the raw data post cruise.

During earlier cruises an equipment setup was used with the EM2040 connected to its own Kongsberg Seapath380 navigation and attitude processing unit with associated GNSS antennas and an MRU5+ motion reference unit mounted on the transducer pod. However, experience during these earlier cruises has shown that the vibration of the ship's deployment pole is too fast for the MRU to be able

to compensate for this motion. This resulted in a cascading of errors. Because of this, during the present cruise it was decided to use the ships Seapath380 in combination with a Kongsberg 3710 DGNSS receiver and ships MRU. Although in theory this would result in data not properly corrected for motion (the pole vibrations is not corrected for) in practice the data was of good enough quality since no accurate bathymetry was needed during this cruise and only water column backscatter data (with backscatter intensity as such being more important than the exact position at which this was measured) was aimed for.
The water column sound velocity profile was determined by means of SVP casts with an AML Oceanographic Base X2. A new cast was done in cases where the sound velocity measured by the sound velocity sensor positioned directly on the echosounder pole, was significantly deviating from the velocity used from the previous cast. The profile was processed with AML seacast software.

3.2 ROV mounted ARIS

(Rosanne Huybens, Laurens van der Marel, Martin Wilpshaar)
The ROV was equipped with an ARIS Explorer 3000 imaging sonar (Figure 2) produced by Sound Metrics. The two main aims of this instrument were 1) detecting the presence of gas seeps and help guiding the ROV towards the seep locations and 2) use the high-resolution images to determine bubble speed and bubble rate fluctuations order to quantify the volume of gas being released within a certain time period at these sites.
The ARIS 3000 Explorer is a high-resolution acoustic imaging instrument using a frequency of 1.8 MHz in detection mode and 3 MHz when in identification mode. The image is constructed from its 128 individual beams. During the cruise the high resolution 3 MHz identification mode was used. This resulted in high quality `acoustic video' data. Because of the high frequency used, the range of the system is limited to about 5 metres in identification mode. However, since the acoustic signals were not hampered by the very high concentration of suspended material in the water column, limiting the optical visibility often to less than the length of the ROV manipulator arm, it was still possible to produce the needed high-resolution imagery. An example of the quality of the ARIS data can be seen in Figure 4.

Figure 2 The complete ARIS Explorer 3000 equipment. The underwater transducer unit is shown on the right hand side (size about 30x18x14 cm). Image by Sound Metrics.

When interpreting ARIS images, in needs to be considered that the sonar produces a two dimensional image of a three-dimensional world (Figure 3). In addition to this, because the positioning of the ROV relative to the seep site can be limited due to wave (shallow water and sometimes strong wave action during the cruise, waves can influence conditions at the seabed) and tidal current conditions it was not always possible to have an optimal orientation of the acoustic camera which could result in non-optimal imaging orientations. In addition to this, one has to realise that the `viewing direction' of the camera is not the same as the viewing direction of the observer watching the screen (Figure 4).

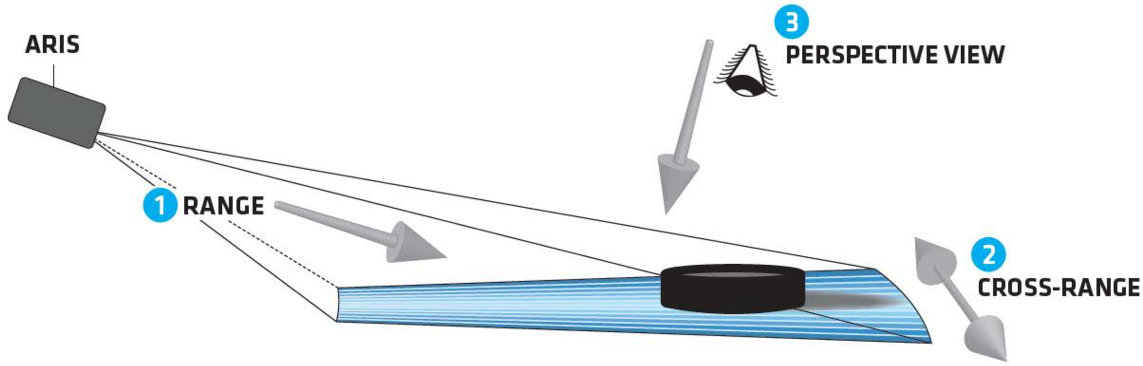

Figure 3 Image illustrating the viewing direction of the ARIS 3000 and the perspective view of the observer. Image bt Sound Metrics.

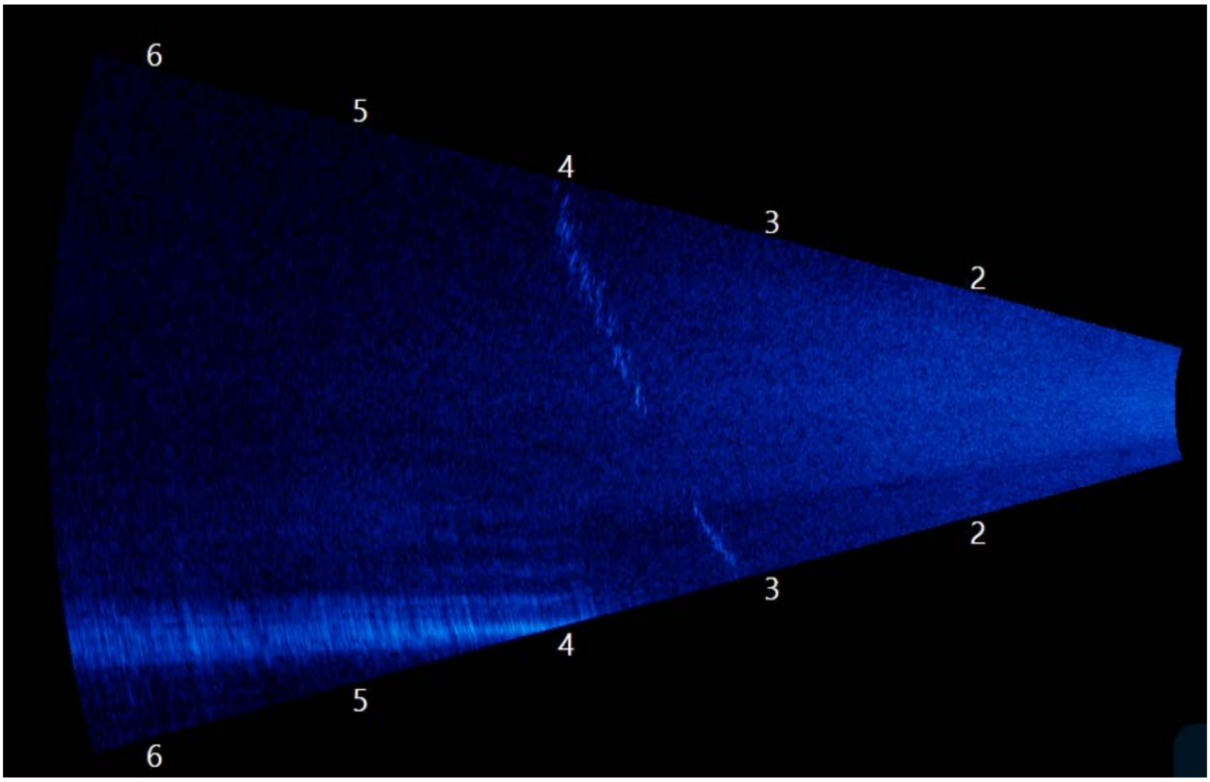

Figure 4 Screenshot of the ARIS 3000 as an example of the data quality produced by the system. An intermittent bubble stream can clearly be observed in the centre of the image. The seabed is represented by the bright blue horizontal line.

3.3 ROV mounted funnel

A small, 'handheld' funnel with an attached syringe (Figure 5) was in some cases attached to the ROV for dives (Figure 6). It was used when bubble plumes were located to measure the flux. To do so the ROV would fly to a bubble plume and put the funnel over the plume. By aiming the ROV's camera at the funnel the filling of the syringe could be watched. The times and volumes were noted on observation sheets to later calculate flux.

Figure 5 The funnel has a syringe attached on top to measure volumes.

Figure 6 ROV inside TMS on deck, funnel is mounted to arm on the right.

3.4 Bubble generator

To contribute to the knowledge of how to accurately quantify methane leakage acoustically, a series of experiments using a controlled gas leak at the seabed have been conducted. These experiments aimed to calibrate multibeam echosounder (MBES) signals against known gas release rates and were realised through the development of a custom bubble generator by the NIOZ workshop. The built bubble generator produced a steady stream of distinct air bubbles, while also allowing the release rate to be precisely controlled. With the addition of a sparger on top of the air outlet, the bubble size distribution of the released gas was adjusted in an attempt to achieve a consistent and predefined bubble size. Eventually, the bubble generator was equipped with a GoPro aimed at the sparger/ bubble release point as well.

When deployed successfully, the bubble generator was left on the seabed. Before every MBES operation both ARIS and ROV mounted funnel measurements were conducted, so that with every variation in flow rate setting both the bubble size and flow rate could be determined. As the location of the bubble generator was recorded during deployment, it was made sure that the Pelagia sailed directly over the generator during the multibeam echosounder operations.

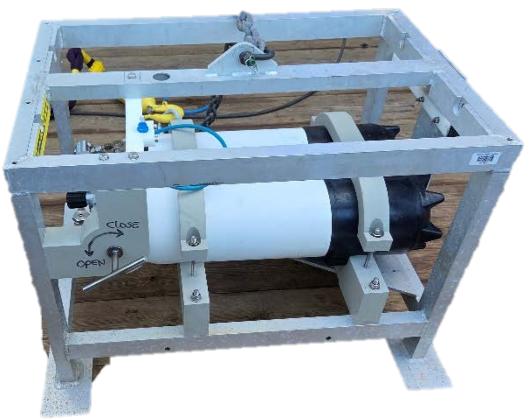

Figure 8 Bubble generator on deck, ready for deployment

Figure 7 ROV camera view of the bubble generator placed on the seabed. Flow rate measurement funnel is located in the right hand.

Within the study area, experiments with the bubble generator were conducted at three locations: at a depth of 30 meters, 46 meters and 43 meters. During the experiments at this last location, a leaking well was present, and its bubble plume could be investigated in combination with the bubble generator's plume.
In the end, 45 MBES measurement were recorded where bubble plumes could be seen clearly in the water column data. The returned acoustic signals obtained from these 45 measurements correspond to seven distinct flow rates. By systematically comparing these measured signals with the corresponding known gas release rates, a field-based calibration curve will be established. The established quantitative relationship enables more precise evaluation of uncertainties and sensitivity es in current water column data-based gas flow estimations.

4. Dissolved Methane in the Water column

Annalisa Delre

4.1 In situ measurements

Along with the standard method consisting of sampling with Niskin bottles, a Methane Sensor Type LMS (Franatech GmbH, Germany, Figure 4.1) was used to measure dissolved methane concentration in the water column. The detection principle of this device is based on laser absorptiometry. Water is pumped across the laser cavities membrane with a Seabird 5M Titanium pump. The dissolved methane in the water diffuses through a silicon-rubber membrane into the measuring chamber. Absorption of laser light was then proportional to the mixing ratio of methane in the instrument's measuring chamber, which was in equilibrium with dissolved methane in the sea water. With the aid of a factory calibration, the mixing ratio in the cavity was corrected for the inertia of the silicon membrane, allowing to calculate water column methane concentration (Wiesenburg et al., 1979). The sensor was installed in the frame of the CTD carousel and measured during each cast. The same sensor was installed on the mini-lander frame (see respective section in the cruise report).

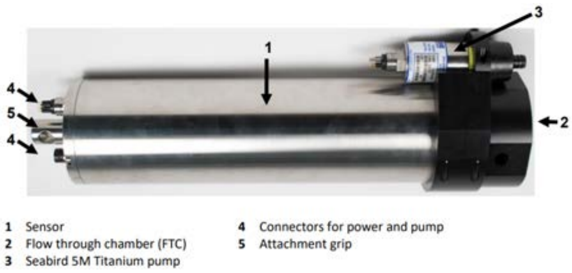

Figure 4.1 The Methane Sensor.

4.2 Discrete water samples

We performed casts with a conductivity-temperature-depth (CTD) probe at two interesting locations (station 28 and 91). Considering the water column well mixed, we decided to collect distinct samples at 3 depth: bottom, middle and surface. Dissolved methane concentrations were determined using a headspace (HS) technique (Green, 2005). As soon as CTD was in the deck, 260 ml glass serum bottles were filled in triplicates from the Niskin bottles, closed with black-butyl rubber stoppers (Rubber B.V., the Netherlands) and crimped top-sealed. Subsequently, 10ml N_2 was added to create a headspace and we fixed the sample with 5ml NaOH solution (25% w/v). The methane concentrations in the headspace will be measured in our home laboratory with a gas-chromatograph (Thermo Scientific FOCUS GC equipped with a Restek stainless steel column HayeSep-Q, 80/100, General configuration (length 2 m, 2 mm i.d., 1/8 in. o.d.) with flame ionization detection.

Bibliography

Green, J. D.: Headspace analysis Static, in: Encyclopedia of Analytical Science (Second Edition), edited by: Worsfold, P., Townshend, A., and Poole, C., Elsevier, Oxford, 229–236, https://doi.org/10.1016/B0-12-369397-7/00254-5, 2005.

Wiesenburg, D. A., & Guinasso Jr, N. L. (1979). Equilibrium solubilities of methane, carbon monoxide, and hydrogen in water and sea water. Journal of chemical and engineering data, 24(4), 356-360.

5. Autonomous lander systems for long-term monitoring

Two autonomous landers were used during the cruise to measure at bubble plumes for a prolonged period. The Mini-lander (or M-lander) was deployed for two days while the Funnel Lander (or F-lander) was deployed as long as possible to cover multiple tidal cycles and natural variances in methane flux. The F-lander was used to catch bubbles and measure fluxes, while the Mini-lander was used to measure multiple parameters.

5.1 Mini-Lander

Annalisa Delre, Rosanne Huybens

An autonomous lander frame was developed by NIOZ that was equipped with multiple to enable long-term timelapse measurements and recordings. For the PE-537 cruise an M-lander was developed (Figure 9). The reason to do so was that it proved to be difficult to accurately place the previously used Albex lander, while the M-lander could be dragged in place by the ROV. The lander was equipped with a laser absorption spectrometer to measure the amount of dissolved methane in the water, a doppler current profiler, hydrophone and a CTD sensor (Conductivity, Temperature, Depth) (Table 1). The spectrometer was powered by a 15V battery-pack that was attached to the lander. The rest of the sensors were powered by internal batteries.

During the PE-549 cruise the M-lander was deployed one time at one locations, namely at a natural seepage location near well B17-04. Before lander deployment, the bubble plume locations were determined with the multibeam. Based on the plume locations, the lander was deployed as close as possible with respect to the bubble plumes and dragged in its final position by the ROV. After deployment of two days, the lander was retrieved and the data from each sensor was collected.

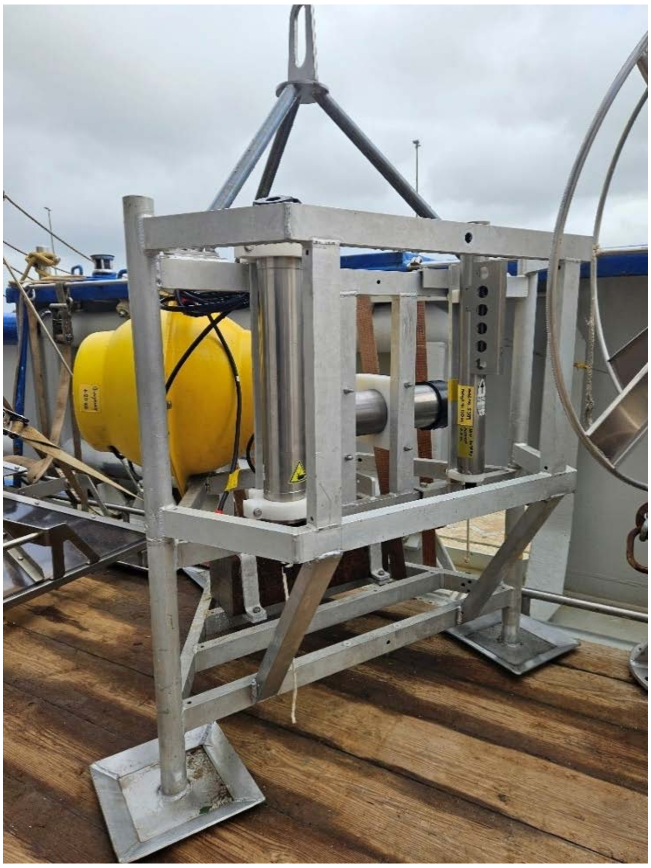

Figure 9 Mini-lander on deck

Table 1 Equipment mounted to the mini-lander with the used configurations during PE-549

Equipment	Model	Serial number	Software
Current profiler	Nortek Aquadopp current profiler	05-10618	Aquapro V20.00.02
Hydrophone	icListen 200 SC2-ETH	6083	Lucy
Laser spectrometer	Franatech	05-10618	Franatech Datalogger Support
CTD	Microcat CTD SBE37	5389	Sea Term V1.59

5.1.1 Current profiler (Aquapro)

The Nortek Aquadopp current profiler (Aquapro) measures current speed and direction in multiple layers, or vertical cells, through the water column. The idea of vertical cells is that the currents vary little in the horizontal plane, but may differ more in vertical layers due to for instance the tidal cycles. An acoustic Doppler instrument transmits a short pulse of sound ("ping") of constant frequency into the water, listens to its echo and measures the change in pitch or frequency of the echo caused by the doppler effect. The temperature is measured by a thermistor embedded in the head and reported in degrees Celsius. This information is of vital importance, since the instrument uses the speed of sound to convert time to distance, and the speed of sound depends on temperature. Furthermore, the hydrostatic pressure is measured with the pressure sensor and reports in units of dbar.

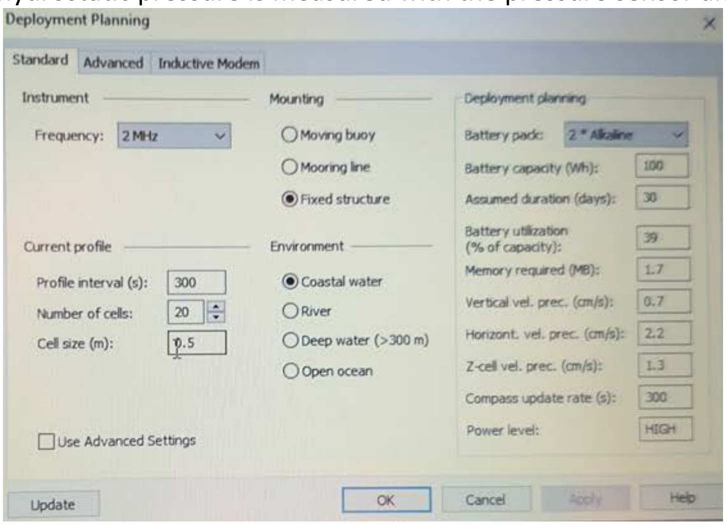

Figure 10 Settings of the Aquadopp current profiler

During PE-549, the current profiler was mounted on the lander with the transducer head facing upward and level with the top of the frame, so that it has an unobstructed 'view' into the overlying water column. During the deployment of the lander, every 5 minutes the current and direction was measured over 20 cells of each 0.5 m, covering a water column of 10 m. Also, the pressure and temperature at the instrument was measured every 5 minutes.

5.1.2 Hydrophone

A hydrophone (Figure 11) was used to record the sound of the bubbles. The goal of these recordings is to relate sound to the number of bubbles in the water column. Sound is recorded continuously. The hydrophone was added to the lander last minute. Therefore, it was not possible to also install the 24V battery pack that was needed to record during the whole deployment. The internal battery powered measurements for roughly eleven hours.

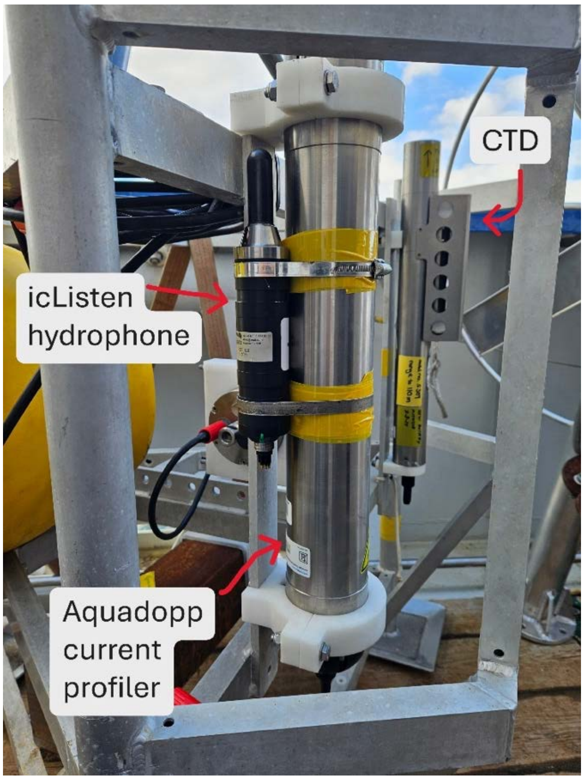

Figure 11 Mini-lander with hydrophone, Aquadopp and CTD mounted to it.

5.1.3 Laser spectrometer

A Methane Sensor Type LMS (Franatech GmbH, Germany, Figure 11) was attached to the lander frame (see section 4). The LMS was preprogrammed to sample every 30 seconds.

5.1.4 CTD (MicroCAT)

The SBE 37-SM MicroCAT (CTD) (Figure 12) is a sensor that measures water parameters in one location over an extended period to produce a time-series of data. It measures the Conductivity (S/m), Temperature (°C) and pressure (dbar), from which the variable salinity and sound velocity of the seawater can be derived. During the PE-549 expedition the MicroCAT was fixed vertically in the top part of the lander. During deployment every 5 minutes the conductivity, temperature and pressure were measured and from which salinity was derived.


Figure 12 CTD MicroCAT

5.2 F-Lander

Rosanne Huybens

The Funnel Lander (F-Lander; Figure 13) is a lander that was developed for expedition PE537 and consists of a large funnel (1,5 by 1,5 m) that catches bubbles and guides them into a measuring chamber. One adjustment was made relative to the PE537 expedition, namely the sensors were replaced to optical sensors that notice the light refraction difference between seawater and gas. The time it takes to fill the chamber is measured. The measuring chamber is 4661.67 ml in volume and when it is full, the captured gas is automatically released, and the time of release is recorded. From this we can compute the flux in ml per second. Secondly, the lander is equipped with a MicroCAT CTD (similar to the one on the m-lander, with S/N 26615). The CTD records conductivity, depth and temperature, and this allows for conversion of the measured volume into moles and grams (using the formula pV = nRT). This results in a flux in gram per second.

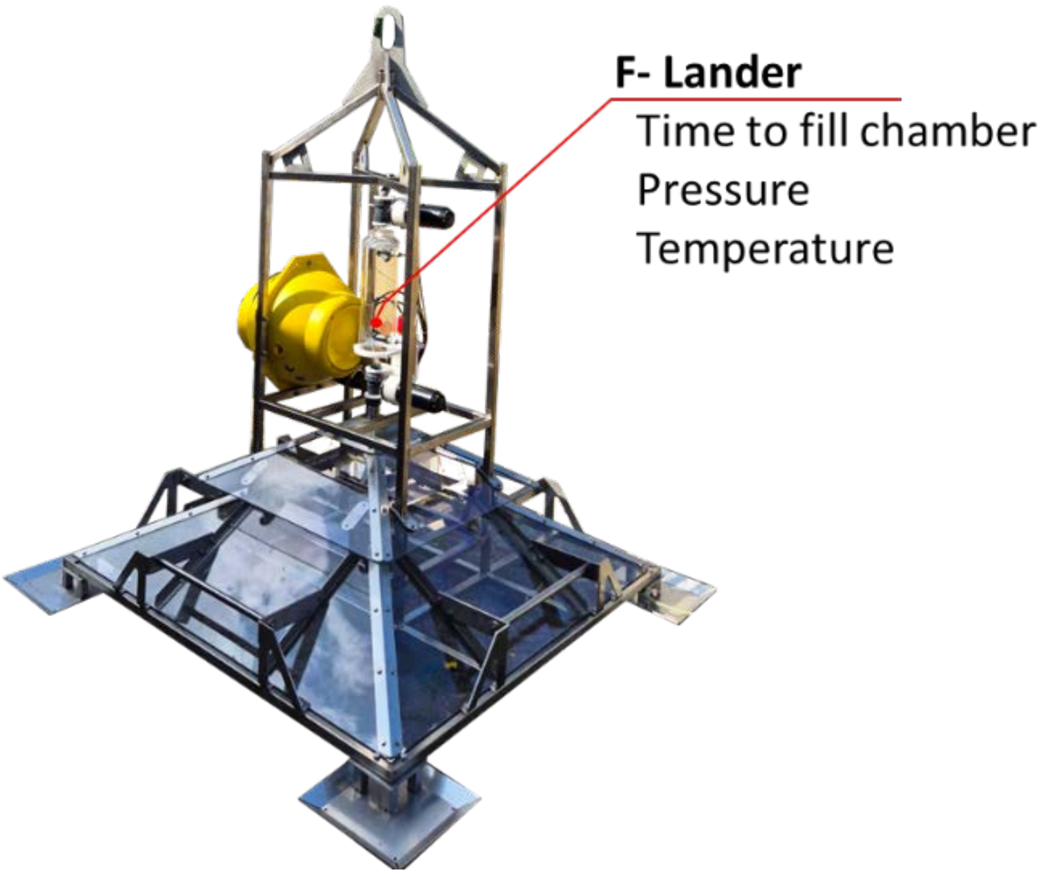

Figure 13 The funnel lander

Appendix I Station list

Date	latitude	longitude	Phase name	Device name	Action name	Operation Id	Cast	Location
22/09/2025 11:45	**52.9958**	**4.7952**	None 0	None	CRUISE START	64PE549	None	Marsdiep
23/09/2025 09:36	**55.0318**	**4.4833**	STATION 2	Multibeam	BEGIN	64PE549EM3022	2_1	**B17-04**
23/09/2025 10:15	**55.0363**	**4.4808**	TRANSIT 3	Multibeam	END	64PE549EM3022	2_1	
23/09/2025 14:59	**55.0117**	**4.5108**	STATION 3	ROV deployment	FAIL	64PE549ROVDEP3	3_1	
23/09/2025 17:12	**54.746**	**4.8485**	STATION 4	SVP	BEGIN	64PE5494	4_1	**F06-06**
23/09/2025 17:40	**54.7448**	**4.8482**	STATION 5	Multibeam	BEGIN	64PE549EM3025	5_1	
23/09/2025 18:48	**54.7513**	**4.8542**	STATION 5	Multibeam	END	64PE549EM3025	5_1	
23/09/2025 19:52	**54.8082**	**4.7102**	STATION 6	SVP	END	64PE5496	6_1	**F06-07**
23/09/2025 19:59	**54.8065**	**4.7102**	STATION 7	Multibeam	BEGIN	64PE549EM3027	7_1	
23/09/2025 21:14	**54.8107**	**4.7108**	STATION 7	Multibeam	END	64PE549EM3027	7_1	
23/09/2025 22:09	**54.827**	**4.6772**	STATION 8	Multibeam	BEGIN	64PE549EM3028	8_1	**F06-01**
23/09/2025 23:24	**54.8307**	**4.6792**	STATION 8	Multibeam	END	64PE549EM3028	8_1	
24/09/2025 00:16	**54.853**	**4.6557**	STATION 9	Multibeam	BEGIN	64PE549EM3029	9_1	**F02-01**
24/09/2025 01:45	**54.8575**	**4.6593**	STATION 9	Multibeam	END	64PE549EM3029	9_1	

24/09/2025 02:30	**54.9142**	**4.6072**	STATION 10	Multibeam	BEGIN	64PE549EM30210	10_1	**F02-07**
24/09/2025 04:07	**54.9482**	**4.603**	STATION 10	Multibeam	END	64PE549EM30210	10_1	
24/09/2025 06:07	**55.0335**	**4.4813**	STATION 11	ROV deployment	BEGIN	64PE549ROVDEP11	11_2	**B17-04**
025-09-24 08:14:56	**55.034**	**4.4803**	STATION 11	Mini Lander	END	64PE54911	11_1	
24/09/2025 08:14	**55.034**	**4.4803**	STATION 11	ROV deployment	END	64PE549ROVDEP11	11_2	
24/09/2025 11:27	**54.9313**	**4.8625**	STATION 12	SVP	END	64PE54912	12_2	**F03-09**
24/09/2025 11:04	**54.9327**	**4.855**	STATION 12	Multibeam	BEGIN	64PE549EM30212	12_1	
24/09/2025 13:11	**54.9323**	**4.8633**	STATION 12	Multibeam	END	64PE549EM30212	12_1	
24/09/2025 13:25	**54.9358**	**4.8615**	STATION 13	Multibeam	BEGIN	64PE549EM30213	13_1	**F03-02**
24/09/2025 14:44	**54.9377**	**4.85**	STATION 13	Multibeam	END	64PE549EM30213	13_1	
24/09/2025 14:44	**54.9377**	**4.85**	TRANSIT 14	ROV deployment	BEGIN	64PE549ROVDEP13	13_2	
24/09/2025 15:18	**54.9375**	**4.851**	TRANSIT 14	ROV deployment	END	64PE549ROVDEP13	13_2	
24/09/2025 15:54	**54.9805**	**4.9452**	STATION 14	Multibeam	BEGIN	64PE549EM30214	14_1	**F03-07**
24/09/2025 16:49	**54.9818**	**4.9523**	STATION 14	Multibeam	END	64PE549EM30214	14_1	
24/09/2025 17:23	**54.9858**	**4.9023**	STATION 15	Multibeam	BEGIN	64PE549EM30215	15_1	**F03-FA-01**
24/09/2025 18:02	**54.9868**	**4.903**	STATION 15	Multibeam	END	64PE549EM30215	15_1	
24/09/2025 18:15	**54.9917**	**4.8997**	STATION 16	Multibeam	BEGIN	64PE549EM30216	16_1	**F03-08**
24/09/2025 19:08	**54.993**	**4.9052**	STATION 16	Multibeam	END	64PE549EM30216	16_1	

24/09/2025 19:29	**54.9923**	**4.8992**	STATION 17	Multibeam	BEGIN	64PE549EM30217	17_1	**F03-01**
24/09/2025 20:36	**55.0013**	**4.904**	STATION 17	Multibeam	END	64PE549EM30217	17_1	
24/09/2025 20:39	**55.0025**	**4.903**	STATION 18	Multibeam	BEGIN	64PE549EM30218	18_1	**B18-03**
24/09/2025 21:37	**55.0058**	**4.9112**	STATION 18	Multibeam	END	64PE549EM30218	18_1	
24/09/2025 22:56	**55.0452**	**4.7267**	STATION 19	Multibeam	BEGIN	64PE549EM30219	19_1	**B18-06**
25/09/2025 00:26	**55.0448**	**4.7388**	STATION 19	Multibeam	END	64PE549EM30219	19_1	
25/09/2025 01:51	**55.0217**	**4.5095**	STATION 20	Multibeam	BEGIN	64PE549EM30220	20_1	**B17-03 → B17-05**
25/09/2025 03:48	**55.0295**	**4.5255**	STATION 20	Multibeam	END	64PE549EM30220	20_1	
25/09/2025 06:06	**55.0347**	**4.4767**	STATION 21	SVP	BEGIN	64PE54921	21_1	**B17-04**
25/09/2025 06:11	**55.0345**	**4.4777**	STATION 21	SVP	END	64PE54921	21_1	
25/09/2025 06:20	**55.034**	**4.4762**	STATION 21	Multibeam	BEGIN	64PE549EM30221	21_2	
25/09/2025 08:14	**55.035**	**4.4867**	STATION 21	Multibeam	END	64PE549EM30221	21_2	
25/09/2025 08:55	**55.0303**	**4.5228**	STATION 22	ROV deployment	BEGIN	64PE549ROVDEP22	22_1	**B17-05**
25/09/2025 13:24	**55.0312**	**4.5232**	STATION 22	Funnel Lander	END	64PE54922	22_2	
25/09/2025 13:44	**55.0313**	**4.5232**	STATION 22	ROV deployment	END	64PE549ROVDEP22	22_1	
25/09/2025 15:10	**55.0337**	**4.4828**	STATION 23	ROV deployment	BEGIN	64PE549ROVDEP23	23_1	**B17-04**
25/09/2025 15:15	**55.0337**	**4.4843**	STATION 23	ROV deployment	END	64PE549ROVDEP23	23_1	
25/09/2025 15:34	**55.0335**	**4.4903**	STATION 24	Multibeam	BEGIN	64PE549EM30224	24_1	**B17-04 box**

25/09/2025 23:45	**55.0407**	**4.4955**	STATION 24	Multibeam	END	64PE549EM30224	24_1	
26/09/2025 00:28	**55.0247**	**4.5092**	STATION 25	Multibeam	BEGIN	64PE549EM30225	25_1	**B17-03**
26/09/2025 01:25	**55.0222**	**4.5168**	STATION 25	Multibeam	END	64PE549EM30225	25_1	
26/09/2025 06:40	**55.0198**	**4.5063**	STATION 26	SVP	BEGIN	64PE54926	26_1	**B1705 box**
26/09/2025 06:41	**55.02**	**4.5062**	STATION 26	SVP	END	64PE54926	26_1	
26/09/2025 13:45	**55.0335**	**4.4805**	STATION 27	Mini Lander	RECOVER	64PE54927	27_1	**B17-04**
26/09/2025 14:39	**55.0335**	**4.4805**	STATION 28	CTD with Samples	BOT	64PE549CTDBOT28	28_1	
26/09/2025 17:26	**55.0272**	**4.5305**	STATION 29	Multibeam	BEGIN	64PE549EM30229	29_1	**B17-05**
26/09/2025 20:58	**55.0327**	**4.514**	STATION 29	Multibeam	END	64PE549EM30229	29_1	
26/09/2025 21:35	**55.024**	**4.4963**	STATION 30	Multibeam	BEGIN	64PE549EM30230	30_1	**B17-03**
27/09/2025 05:46	**55.0305**	**4.5218**	STATION 30	Multibeam	END	64PE549EM30230	30_1	
27/09/2025 07:58	**55.0305**	**4.5228**	STATION 32	F lander salvage	BEGIN	64PE54932	32_3	
27/09/2025 12:07	**55.0313**	**4.5233**	STATION 32	F lander salvage	END	64PE54932	32_3	
27/09/2025 14:58	**54.7893**	**4.481**	TRANSIT 34	SVP	END	64PE54932	32_4	**F05-01**
27/09/2025 14:59	**54.7895**	**4.4808**	TRANSIT 35	Multibeam	BEGIN	64PE549EM30233	33_1	
27/09/2025 15:48	**54.7838**	**4.4882**	TRANSIT 35	Multibeam	END	64PE549EM30233	33_1	
27/09/2025 16:37	**54.745**	**4.5642**	TRANSIT 36	Multibeam	BEGIN	64PE549EM30234	34_1	**F05-04**

27/09/2025 17:16	**54.7415**	**4.5717**	TRANSIT 36	Multibeam	END	64PE549EM30234	34_1	
27/09/2025 18:15	**54.6417**	**4.6378**	STATION 35	Multibeam	BEGIN	64PE549EM30235	35_1	**F08-01**
27/09/2025 19:06	**54.638**	**4.6482**	STATION 35	Multibeam	END	64PE549EM30235	35_1	
27/09/2025 21:55	**54.5508**	**4.0637**	STATION 37	SVP	END	64PE54937	37_1	**F07-01**
27/09/2025 22:22	**54.5512**	**4.054**	STATION 37	Multibeam	BEGIN	64PE549EM30237	37_2	
27/09/2025 23:26	**54.555**	**4.0497**	STATION 37	Multibeam	END	64PE549EM30237	37_2	
28/09/2025 00:15	**54.6125**	**3.9447**	STATION 38	Multibeam	BEGIN	64PE549EM30238	38_1	**E09-01**
28/09/2025 01:31	**54.6073**	**3.9507**	STATION 38	Multibeam	END	64PE549EM30238	38_1	
28/09/2025 03:12	**54.403**	**3.7842**	STATION 39	SVP	END	64PE54939	39_1	**E12-04**
28/09/2025 03:24	**54.4028**	**3.7835**	STATION 40	Multibeam	BEGIN	64PE549EM30240	40_1	
28/09/2025 05:36	**54.4718**	**3.6968**	STATION 41	Multibeam	END	64PE549EM30240	40_1	**E12-03**
28/09/2025 06:34	**54.4015**	**3.5627**	STATION 42	Multibeam	BEGIN	64PE549EM30242	42_1	**E11-01**
28/09/2025 06:38	**54.3995**	**3.5642**	STATION 42	Multibeam	END	64PE549EM30242	42_1	
28/09/2025 07:20	**54.4018**	**3.5625**	STATION 42	Bubble generator	BEGIN	64PE54942	42_4	**close to E11-01**
28/09/2025 08:47	**54.401**	**3.5628**	STATION 42	Multibeam	BEGIN	64PE549EM30242	42_5	
28/09/2025 12:03	**54.4022**	**3.5625**	STATION 42	ROV deployment	DEP	64PE549ROVDEP42	42_6	
28/09/2025 14:08	**54.403**	**3.565**	STATION 42	Multibeam	BEGIN	64PE549EM30242	42_7	

28/09/2025 20:02	**54.1295**	**3.887**	STATION 43	Multibeam	BEGIN	64PE549EM30243	43_2	**E18-01**
28/09/2025 20:58	**54.125**	**3.8823**	STATION 43	Multibeam	END	64PE549EM30243	43_2	
28/09/2025 21:42	**54.0802**	**4.007**	STATION 44	Multibeam	BEGIN	64PE549EM30244	44_1	**F16-05**
28/09/2025 22:57	**54.0738**	**4.0062**	STATION 44	Multibeam	END	64PE549EM30244	44_1	
29/09/2025 00:16	**53.9448**	**4.1417**	STATION 45	Multibeam	BEGIN	64PE549EM30245	45_1	**L01-01**
29/09/2025 01:30	**53.9412**	**4.1383**	STATION 45	Multibeam	END	64PE549EM30245	45_1	
29/09/2025 02:17	**53.9103**	**4.2468**	STATION 46	SVP	END	64PE54946	46_1	**L01-03**
29/09/2025 02:17	**53.9103**	**4.2468**	STATION 47	Multibeam	BEGIN	64PE549EM30247	47_1	
29/09/2025 03:28	**53.9008**	**4.2182**	STATION 47	Multibeam	END	64PE549EM30247	47_1	
29/09/2025 03:29	**53.9005**	**4.2167**	STATION 48	Multibeam	BEGIN	64PE549EM30248	48_1	**L01-02**
29/09/2025 04:05	**53.8993**	**4.2235**	STATION 48	Multibeam	END	64PE549EM30248	48_1	
29/09/2025 04:45	**53.8758**	**4.2472**	STATION 49	Multibeam	BEGIN	64PE549EM30249	49_1	**L01-05**
29/09/2025 05:23	**53.8752**	**4.2535**	STATION 49	Multibeam	END	64PE549EM30249	49_1	
29/09/2025 06:25	**53.8485**	**4.0313**	STATION 50	SVP	END	64PE54950	50_1	**L01-04**
29/09/2025 07:24	**53.8433**	**4.0345**	STATION 50	Multibeam	BEGIN	64PE549EM30250	50_2	
29/09/2025 07:24	**53.8433**	**4.0345**	STATION 50	Multibeam	END	64PE549EM30250	50_2	
29/09/2025 07:56	**53.8115**	**3.9952**	STATION 51	Multibeam	BEGIN	64PE549EM30251	51_1	**K06-01**
29/09/2025 09:58	**53.8168**	**3.9828**	STATION 51	Multibeam	END	64PE549EM30251	51_1	

29/09/2025 10:07	**53.8165**	**3.9823**	STATION 51	ROV deployment	DEP	64PE549ROVDEP51	51_2	
29/09/2025 10:34	**53.8163**	**3.9808**	STATION 51	ROV deployment	END	64PE549ROVDEP51	51_2	
29/09/2025 11:20	**53.8152**	**3.9847**	STATION 51	ROV deployment	DEP	64PE549ROVDEP51	51_3	
29/09/2025 11:39	**53.8152**	**3.9847**	STATION 51	ROV deployment	END	64PE549ROVDEP51	51_3	
29/09/2025 12:16	**53.786**	**3.9063**	STATION 52	Multibeam	BEGIN	64PE549EM30252	52_1	**K06-06**
29/09/2025 13:10	**53.7895**	**3.9013**	STATION 52	Multibeam	END	64PE549EM30252	52_1	
29/09/2025 13:43	**53.7582**	**3.8692**	STATION 53	SVP	END	64PE54953	53_1	**K06-08**
29/09/2025 13:48	**53.7585**	**3.869**	STATION 53	Multibeam	BEGIN	64PE549EM30253	53_2	
29/09/2025 15:30	**53.741**	**3.6553**	STATION 53	Multibeam	END	64PE549EM30253	53_2	
29/09/2025 15:45	**53.7382**	**3.6167**	STATION 54	Multibeam	BEGIN	64PE549EM30254	54_1	**K05-F-02, K05-F-03, K05-11**
29/09/2025 16:35	**53.7417**	**3.6155**	STATION 54	Multibeam	END	64PE549EM30254	54_1	
29/09/2025 17:17	**53.6522**	**3.6032**	STATION 55	Multibeam	BEGIN	64PE549EM30255	55_1	**K08-14**
29/09/2025 18:09	**53.6607**	**3.6047**	TRANSIT 57	Multibeam	END	64PE549EM30255	55_1	
29/09/2025 18:47	**53.6048**	**3.5648**	STATION 56	Multibeam	BEGIN	64PE549EM30256	56_1	**K08-2**
29/09/2025 19:32	**53.6008**	**3.5632**	STATION 56	Multibeam	END	64PE549EM30256	56_1	
29/09/2025 19:56	**53.5692**	**3.5457**	STATION 57	Multibeam	BEGIN	64PE549EM30257	57_1	**K08-15**
29/09/2025 20:51	**53.562**	**3.5447**	STATION 57	Multibeam	END	64PE549EM30257	57_1	
29/09/2025 21:34	**53.5465**	**3.4775**	STATION 58	Multibeam	BEGIN	64PE549EM30258	58_2	**K08-07**

29/09/2025 22:20	**53.5468**	**3.4738**	STATION 58	Multibeam	END	64PE549EM30258	58_2	
29/09/2025 23:00	**53.5448**	**3.3907**	STATION 59	Multibeam	BEGIN	64PE549EM30259	59_1	**K08-08**
30/09/2025 00:04	**53.5503**	**3.3903**	STATION 59	Multibeam	END	64PE549EM30259	59_1	
30/09/2025 00:15	**53.5513**	**3.4028**	STATION 60	Multibeam	BEGIN	64PE549EM30260	60_1	**K08-01**
30/09/2025 01:11	**53.5553**	**3.4048**	STATION 60	Multibeam	END	64PE549EM30260	60_1	
30/09/2025 01:55	**53.5033**	**3.43**	STATION 61	Multibeam	BEGIN	64PE549EM30261	61_1	**K08-03**
30/09/2025 02:38	**53.4998**	**3.428**	TRANSIT 63	Multibeam	END	64PE549EM30261	61_1	
30/09/2025 03:16	**53.4472**	**3.3487**	STATION 62	Multibeam	BEGIN	64PE549EM30262	62_1	**K11-02, K11-FA-101, K11-FA-102, K11-FA-103**
30/09/2025 04:30	**53.454**	**3.3402**	STATION 62	Multibeam	END	64PE549EM30262	62_1	
30/09/2025 05:07	**53.3995**	**3.417**	STATION 63	Multibeam	BEGIN	64PE549EM30263	63_1	**K11-03**
30/09/2025 05:42	**53.4035**	**3.4182**	STATION 63	Multibeam	END	64PE549EM30263	63_1	
30/09/2025 06:26	**53.4022**	**3.2837**	STATION 64	SVP	END	64PE54964	64_1	
30/09/2025 06:51	**53.4007**	**3.287**	STATION 64	Multibeam	BEGIN	64PE549EM30264	64_2	**K10-C-01, K10-C-02, K10-C-03, K10-C-04**
30/09/2025 07:42	**53.408**	**3.2873**	STATION 64	Multibeam	END	64PE549EM30264	64_2	
30/09/2025 10:24	**53.408**	**3.2875**	STATION 65	ROV deployment	REC	64PE549ROVDEP65	65_1	**close to K10-C01**
30/09/2025 07:54	**53.408**	**3.2873**	STATION 65	Bubble generator	BEGIN	64PE54965	65_2	
30/09/2025 11:09	**53.408**	**3.2892**	STATION 65	Multibeam	BEGIN	64PE549EM30265	65_4	
30/09/2025 12:04	**53.4083**	**3.2873**	STATION 65	Multibeam	END	64PE549EM30265	65_4	

30/09/2025 14:07	**53.4082**	**3.2872**	STATION 65	Bubble generator	BEGIN	64PE54965	65_6	
30/09/2025 14:34	**53.4075**	**3.2872**	STATION 65	Multibeam	BEGIN	64PE549EM30265	65_7	
30/09/2025 14:55	**53.4082**	**3.2875**	STATION 65	Multibeam	END	64PE549EM30265	65_7	
30/09/2025 15:46	**53.4083**	**3.2872**	STATION 65	Bubble generator	END	64PE54965	65_6	
30/09/2025 20:59	**53.3628**	**3.2478**	STATION 66	SVP	BEGIN	64PE54966	66_1	**K10-B-01, K10-B-02, K10-B-03, K10-B-04, K10-B-05, K10-B-06, K10-B-07, K10-B-08, K10-B**
30/09/2025 21:23	**53.3613**	**3.2565**	STATION 66	Multibeam	BEGIN	64PE549EM30266	66_2	
30/09/2025 22:13	**53.3625**	**3.2498**	STATION 66	Multibeam	END	64PE549EM30266	66_2	
30/09/2025 22:56	**53.3092**	**3.2172**	STATION 67	Multibeam	BEGIN	64PE549EM30267	67_1	**K13-CF-01, K13-CF-02, K13-CF-03, K13-05, K13-CF-05, K13-CF-06**
30/09/2025 23:58	**53.31**	**3.2103**	STATION 67	Multibeam	END	64PE549EM30267	67_1	
01/10/2025 00:37	**53.2823**	**3.21**	STATION 68	Multibeam	BEGIN	64PE549EM30268	68_1	**K13-DE-01, K13-DE-02, K13-DE-03, K13-DE-04, K13-DE-05**
01/10/2025 01:23	**53.2795**	**3.2133**	STATION 68	Multibeam	END	64PE549EM30268	68_1	
01/10/2025 03:53	**53.2863**	**3.8095**	TRANSIT 70	SVP	END	64PE54968	68_2	**K15-14**
01/10/2025 03:54	**53.2862**	**3.8095**	STATION 69	Multibeam	BEGIN	64PE549EM30269	69_1	
01/10/2025 04:46	**53.283**	**3.8065**	STATION 69	Multibeam	END	64PE549EM30269	69_1	
01/10/2025 05:39	**53.2185**	**3.9483**	STATION 70	Multibeam	BEGIN	64PE549EM30270	70_1	**K15-15**
01/10/2025 06:53	**53.2165**	**3.9712**	STATION 70	Multibeam	END	64PE549EM30270	70_1	
01/10/2025 07:13	**53.2168**	**3.9902**	STATION 71	Multibeam	BEGIN	64PE549EM30271	71_1	**K15-09**
01/10/2025 08:10	**53.2172**	**3.9928**	STATION 71	Multibeam	END	64PE549EM30271	71_1	

01/10/2025 09:04	**53.1515**	**3.9488**	STATION 72	SVP	END	64PE54972	72_1	**K18-07**
01/10/2025 09:04	**53.1517**	**3.9488**	STATION 72	Multibeam	BEGIN	64PE549EM30272	72_2	
01/10/2025 11:00	**53.0773**	**3.966**	STATION 73	Multibeam	BEGIN	64PE549EM30273	73_1	**K18-01**
01/10/2025 11:48	**53.0738**	**3.9668**	STATION 73	Multibeam	END	64PE549EM30273	73_1	
01/10/2025 12:22	**53.0702**	**4.0542**	STATION 74	Multibeam	BEGIN	64PE549EM30274	74_1	**L16-15, L16-14**
01/10/2025 13:34	**53.0688**	**4.0573**	STATION 74	Multibeam	END	64PE549EM30274	74_1	
01/10/2025 14:49	**53.2178**	**4.1793**	STATION 75	Multibeam	BEGIN	64PE549EM30275	75_1	**L13-15**
01/10/2025 15:27	**53.2138**	**4.1802**	STATION 75	Multibeam	END	64PE549EM30275	75_1	
02/10/2025 03:56	**55.0325**	**4.524**	STATION 76	Funnel Lander	BEGIN	64PE54976	76_1	**B17-05**
02/10/2025 04:18	**55.0307**	**4.5235**	STATION 76	Funnel Lander	END	64PE54976	76_1	
02/10/2025 06:22	**55.0295**	**4.5235**	STATION 77	ROV deployment	BEGIN	64PE549ROVDEP77	77_2	
02/10/2025 06:48	**55.0297**	**4.5233**	STATION 77	Bubble generator	BEGIN	64PE54977	77_3	
02/10/2025 07:45	**55.0313**	**4.5213**	STATION 77	Multibeam	BEGIN	64PE549EM30277	77_4	
02/10/2025 08:48	**55.0322**	**4.5173**	STATION 77	Multibeam	END	64PE549EM30277	77_4	
02/10/2025 09:10	**55.0302**	**4.5232**	STATION 77	ROV deployment	BEGIN	64PE549ROVDEP77	77_5	
02/10/2025 11:42	**55.0298**	**4.5233**	STATION 77	Bubble generator	END	64PE54977	77_3	
02/10/2025 11:47	**55.0297**	**4.5235**	STATION 77	ROV deployment	END	64PE549ROVDEP77	77_5	
06/10/2025 12:04	**53.3913**	**4.3602**	STATION 78	SVP	END	64PE54978	78_1	**L11-01**

06/10/2025 12:04	**53.3913**	**4.3602**	STATION 78	Multibeam	BEGIN	64PE549EM30278	78_2	
06/10/2025 13:27	**53.4227**	**4.3603**	TRANSIT 81	Multibeam	END	64PE549EM30278	78_3	
06/10/2025 13:27	**53.4227**	**4.3603**	STATION 79	Multibeam	BEGIN	64PE549EM30279	79_1	**L11-07**
06/10/2025 14:16	**53.4235**	**4.353**	STATION 79	Multibeam	END	64PE549EM30279	79_1	
06/10/2025 14:55	**53.4243**	**4.2455**	STATION 80	Multibeam	BEGIN	64PE549EM30280	80_1	**L10-08**
06/10/2025 15:27	**53.4225**	**4.2418**	STATION 80	Multibeam	END	64PE549EM30280	80_1	
06/10/2025 16:38	**53.4072**	**4.2117**	STATION 81	Multibeam	BEGIN	64PE549EM30281	81_1	**L10-D-01, L10-D-02, L10-D-03, L10-D-04, L10-D-05**
06/10/2025 16:38	**53.4072**	**4.2117**	STATION 81	Multibeam	END	64PE549EM30281	81_1	
06/10/2025 17:00	**53.3948**	**4.2052**	STATION 82	Multibeam	BEGIN	64PE549EM30282	82_1	**L10-C-01, L10-C-02, L10-C-03, L10-C-04, L10-C-05, L10-C-06**
06/10/2025 17:41	**53.3917**	**4.2**	STATION 82	Multibeam	END	64PE549EM30282	82_1	
06/10/2025 19:33	**53.5645**	**4.5727**	STATION 83	Multibeam	BEGIN	64PE549EM30283	83_1	**L08-09, L08-H-01, L08-H-02**
06/10/2025 20:39	**53.5638**	**4.5628**	STATION 83	Multibeam	END	64PE549EM30283	83_1	
06/10/2025 22:03	**53.6208**	**4.4795**	STATION 84	Multibeam	BEGIN	64PE549EM30284	84_1	**L08-03**
06/10/2025 22:34	**53.6242**	**4.4735**	STATION 84	Multibeam	END	64PE549EM30284	84_1	
06/10/2025 23:09	**53.6388**	**4.5647**	STATION 85	Multibeam	BEGIN	64PE549EM30285	85_1	**L08-P-01, L08-P-02, L08-P-03, L08-P-05**
07/10/2025 00:12	**53.6413**	**4.5648**	STATION 85	Multibeam	END	64PE549EM30285	85_1	
07/10/2025 02:06	**53.5887**	**4.9625**	STATION 86	SVP	END	64PE54986	86_1	**L09-11**

07/10/2025 02:06	**53.5887**	**4.9625**	STATION 87	Multibeam	BEGIN	64PE549EM30287	87_1	
07/10/2025 02:52	**53.585**	**4.9595**	STATION 87	Multibeam	END	64PE549EM30287	87_1	
07/10/2025 03:17	**53.6132**	**4.9392**	STATION 88	Multibeam	BEGIN	64PE549EM30288	88_1	**L09-12**
07/10/2025 04:05	**53.6097**	**4.9408**	STATION 88	Multibeam	END	64PE549EM30288	88_1	
07/10/2025 04:12	**53.6115**	**4.9515**	STATION 89	Multibeam	BEGIN	64PE549EM30289	89_1	**L09-08**
07/10/2025 04:36	**53.616**	**4.9502**	STATION 89	Multibeam	END	64PE549EM30289	89_1	
07/10/2025 05:02	**53.6572**	**4.9267**	STATION 90	Multibeam	BEGIN	64PE549EM30290	90_1	**L09-07**
07/10/2025 05:54	**53.655**	**4.92**	STATION 90	Multibeam	END	64PE549EM30290	90_1	
07/10/2025 07:50	**53.6403**	**4.5627**	STATION 91	ROV deployment	BEGIN	64PE549ROVDEP91	91_1	**L08-P-01, L08-P-02, L08-P-03, L08-P-05**
07/10/2025 09:43	**53.64**	**4.5623**	STATION 91	ROV deployment	END	64PE549ROVDEP91	91_1	
07/10/2025 10:00	**53.6402**	**4.5625**	STATION 91	CTD with Samples	BOT	64PE549CTDBOT91	91_2	
07/10/2025 11:11	**53.64**	**4.5627**	STATION 91	ROV deployment	BEGIN	64PE549ROVDEP91	91_3	
07/10/2025 11:48	**53.6398**	**4.5627**	STATION 91	ROV deployment	END	64PE549ROVDEP91	91_3	
07/10/2025 12:48	**53.717**	**4.6588**	STATION 92	Multibeam	BEGIN	64PE549EM30292	92_1	**L05-07**
07/10/2025 13:42	**53.7158**	**4.6512**	STATION 92	Multibeam	END	64PE549EM30292	92_1	
07/10/2025 17:09	**54.2215**	**4.5942**	STATION 93	Multibeam	BEGIN	64PE549EM30293	93_2	**F14-07**
07/10/2025 17:48	**54.2192**	**4.5868**	STATION 93	Multibeam	END	64PE549EM30293	93_2	
07/10/2025 20:57	**53.8623**	**5.092**	STATION 94	Multibeam	BEGIN	64PE549EM30294	94_2	**M01-03**

07/10/2025 21:53	**53.8608**	**5.0872**	STATION 94	Multibeam	END	64PE549EM30294	94_2	
07/10/2025 22:01	**53.8548**	**5.0873**	STATION 95	Multibeam	BEGIN	64PE549EM30295	95_1	**M01-02**
07/10/2025 22:42	**53.8542**	**5.0933**	STATION 95	Multibeam	END	64PE549EM30295	95_1	
07/10/2025 22:42	**53.8542**	**5.0933**	STATION 95	End of Sci progr.	END			